EPJ Web of Conferences **209**, 01030 (2019) https://doi.org/10.1051/epjconf/201920901030
RICAP-18

Proton energy spectrum with the DAMPE experiment

Antonio De Benedittis[1,2,a] (on behalf of the DAMPE Collaboration)

[1] *Dip.to di Matematica e Fisica "E. De Giorgi", Università del Salento, Via per Arnesano, 73100, Lecce, Italy*
[2] *Istituto Nazionale di Fisica Nucleare (INFN), Sezione di Lecce, Via per Arnesano, 73100, Lecce, Italy*

Abstract. The DAMPE (DArk Matter Particle Explorer) experiment, in orbit since December 17th 2015, is a space mission whose main purpose is the detection of cosmic electrons and photons up to energies of 10 TeV, in order to identify possible evidence of Dark Matter in their spectra. Furthermore it aims to measure the spectra and the elemental composition of the galactic cosmic rays nuclei up to the energy of hundreds of TeV. The proton analysis and the flux with kinetic energy ranging from 50 GeV up to 100 TeV, at the end of two years of data taking, will be presented and discussed.

1 Introduction

Cosmic Rays (CRs) with energies up to $\sim$ 4 PeV (the so called *knee* of the CRs spectrum [1]) are widely to be believed originated by the strong shock of Supernovae explosions in the Milky Way [2]. CRs are mainly composed of protons, therefore a very precise measurement of the proton flux up to energies of the order of PeV is crucial to understand the mechanism at the origin of their acceleration and the physical basis of the *knee*.

Starting from energies higher than 30 GeV the energy spectrum of CRs is expected to follow a featureless power-law according to the conventional acceleration models [3]. Recent measurements of proton flux carried out by baloon- and space-borne experiments (ATIC-2 [4], CREAM I-III [5], AMS-02 [6], PAMELA [7]) observed a spectral *hardening*, that is a deviation from the single power-law distribution. Moreover a spectral *softening* was observed at energies higher than 50 TeV (CREAM I-III [5], NUCLEON [9], ARGO-YBJ [8]).

One of the goals of DAMPE (DArk Matter Particle Explorer) is to investigate with high precision the *hardening* and the *softening* fitting a bridge between direct and indirect measurements.

2 DAMPE detector

The DAMPE detector [10] is composed by four sub-detectors from the top to the bottom: a Plastic Scintillator strip Detector (PSD), a Silicon-Tungsten tracKer-converter (STK), a BGO calorimeter and a NeUtron Detector (NUD).

The PSD measures the absolute value of the charge of incident particles (up to Z$\leq$28), it provides also background rejection for gamma-ray detection. The STK reconstructs the trajectory and gives an independent charge measurement, it also acts as a gamma-ray converter using three tungsten foils

[a] e-mail: antonio.debenedittis@le.infn.it

interleaved in the first layers of silicon strips. The BGO calorimeter measures the energy of the particles and provides an electron/hadron discrimination, his depth (about 32 X_0) ensures that almost 100% of the energy of electrons and γ-rays is deposited in the calorimeter, and about 40% regarding nuclei [11]. The NUD gives a redundant electron/hadron discrimination using the neutrons produced in BGO by the hadronic showers.

3 Data analysis

Two years of data taking since the 1st January, 2016 to the 31st December, 2017 are taken in account in this analysis. The operational live time is about 75.5%, the lost time consists of three part: the instrumental dead time, the crossing time of the South Atlantic Anomaly (SAA) region, the time for the on-orbit calibration procedures.

3.1 Event selection

In this analysis some pre-selection cuts are applied to satisfy some basilar requests: to ensure that all sub-detectors work in good conditions, the SAA events are excluded; to avoid the effect due to the geomagnetic cut-off, only particles that release $E \geq 20$ GeV in the calorimeter are considered; the track of the particle has to be geometrically contained in the detector in order to select particles that are crossing all the sub-detectors.

After the pre-selection cuts, only the events passing the High Energy Trigger (HET), that foresees a deposited energy in the first four layers of BGO higher than 230 MeV ($\sim$ 10 MIPs). The HET efficiency (Fig. 1 *left side*) is estimated using the Unbias Trigger (which requires that the energy deposited in each of the first two BGO layers has to be ≥ 0.5 MIP):

$$\varepsilon_{trig} = \frac{N_{he|unb}}{N_{unb}} \tag{1}$$

where N_{unb} are the events passing the unbias trigger and $N_{he|unb}$ are those that satisfy also the HET.

Moreover only the events with at least a reconstructed track in the STK are selected, and the selected track has to cross all the PSD layers and has to satisfy the STK-BGO match. The track reconstruction efficiency (Fig. 1 *right side*) is estimated using a proton sample selected by an independent charge selection based on the reconstructed shower axis in the calorimeter, and it is defined as:

$$\varepsilon_{track} = \frac{N_{track|BGOtrack}}{N_{BGOtrack}} \tag{2}$$

where $N_{BGOtrack}$ are the events with a selected track in the calorimeter and $N_{track|BGOtrack}$ are those passing the STK track selection cuts.

Finally the proton candidates are selected by the information coming from the PSD charge distribution for different ranges of BGO energy. The charge recostruction efficiency (Fig. 2) is estimated independently for each PSD layer using the information coming from the first STK layer and from the other PSD layer.

3.2 Background

The background for protons is due mainly to mis-identified helium nuclei and electron events. The helium contamination is evaluated applying the template-fit method to the charge distributions obtained from PSD signals and using the MC samples of proton and helium nuclei (Fig. 3 *left side*). The

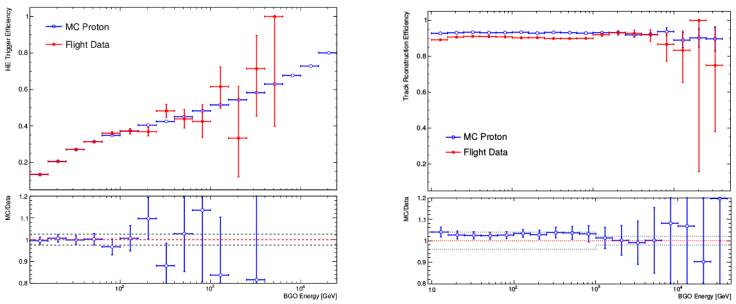

Figure 1. *Left* - The HET efficiency as a function of BGO energy. *Right* - The Track reconstruction efficiency as a function of BGO energy. In both plots the red points are for flight data and the blue points are for MC data.

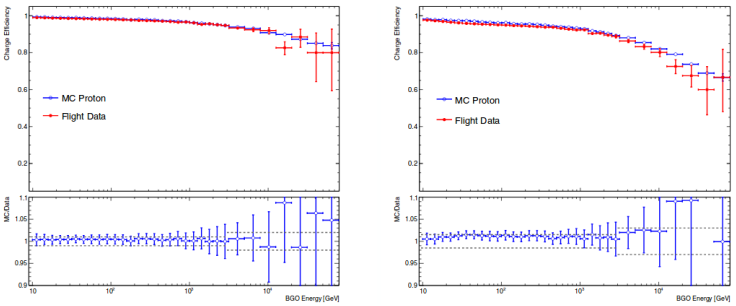

Figure 2. The charge reconstruction efficiency as a function of BGO energy, for PSD layer 1 (*Left*), for PSD layer 2 (*Right*). In both plots the red points are for flight data and the blue points are for MC data.

helium background is less than 2% up to energies of about 10 TeV; while the electron background, thanks to the high e/p discrimination power, is less than 0.1% (Fig. 3 *right side*). The helium and electron contamination is taken into account in the systematic uncertainties.

4 Results and conclusions

The effective acceptance (Fig. 4 *left side*) is evaluated using a MC sample of pure proton events. It is defined (for the *i*-th primary energy bin) as:

$$A_{eff,i} = A_{gen} \times \frac{N_{pass,i}}{N_{gen,i}} \tag{3}$$

where A_{gen} is the geometrical factor of the MC generation half-sphere, $N_{pass,i}$ and $N_{gen,i}$ are the number of generated events and surviving events respectively.

The *right side* of Fig. 4 shows the DAMPE preliminary proton flux as a function of kinetic energy, compared with the previous measurements of AMS-02, PAMELA, ATIC-2, CREAM-III. The spectral hardening at $E \simeq 200$ GeV is in agreement with the measurements of AMS-02 and PAMELA. Moreover a softening at energies higher than 10^4 GeV, according to ATIC and CREAM (within the systematic uncertainties) results, has been observed with unprecedent resolution.

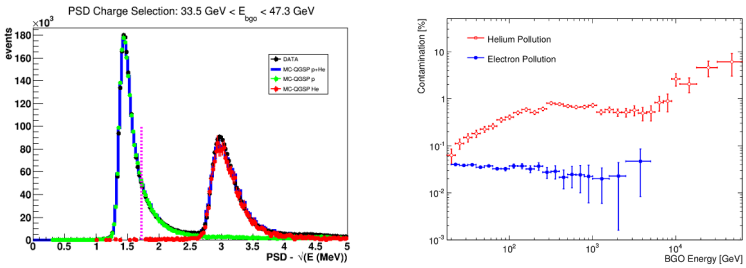

Figure 3. *Left* - The combined charge spectrum of PSD for protons and helium nuclei, for BGO energies between 33.5 GeV and 47.3 GeV. In this plot there are the on-orbit data (black), with the best fit templates of MC protons (green), helium nuclei (red) and their sum (blue). The vertical line shows the cut applied to select proton canditates. *Right* - The fraction of helium background (red) and electron background (blue) in proton candidate events as a function of BGO energy.

The data analysis and the evaluation of systematic uncertainties are still on-going. In the future, with the increase in data sample it is expected to obtain a proton flux up to energies higher than 100 TeV with high precision.

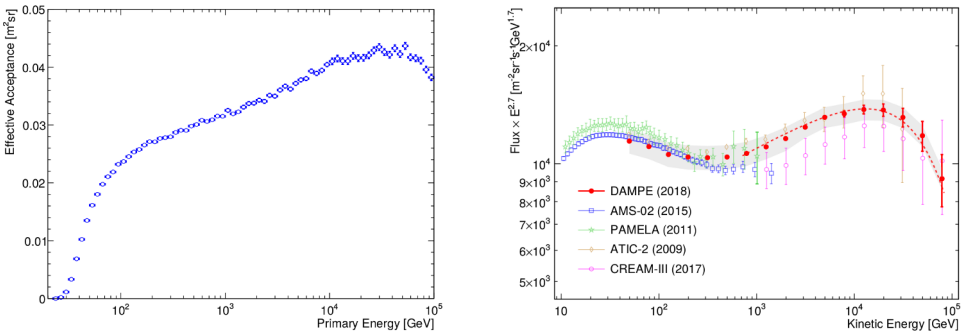

Figure 4. *Left* - The effective acceptance of protons as a function of primary energy. *Right* - The preliminary proton flux times $E^{2.7}$ as a function of primary energy (the shaded area shows the systematic errors).

References

[1] Hoerandel J., Astropart. Phys. **19**, 193–220 (2003).
[2] Baade W., Zwicky F., Phys. Rev., **46**, 76 (1934).
[3] Fermi E., Phys. Rev., **75**, 1169 (1949).
[4] Panov A. D. *et al.* (The ATIC Collaboration), Bull. Rus. Acad. Sci. Phys., **73**, 564 (2009).
[5] Ahn H. S. *et al.* (The CREAM Collaboration), Astrophys. J., **714**, L89 (2010).
[6] Aguilar M. *et al.* (The AMS Collaboration), Phys. Rev. Lett., **114**, 171103 (2015).
[7] Adriani O. *et al.* (The PAMELA Collaboration), Science, **332**, 69 (2011).
[8] Bartoli B. *et al.* (The ARGO-YBJ Collaboration), Phys. Rev. D **92**, 092005 (2015).
[9] Atkin E. *et al.* (The NUCLEON Collaboration), Astropart. Phys. **90**, 69-74 (2017).
[10] Chang J. *et al.* (The DAMPE Collaboration), Astropart. Phys. **95**, 6–24 (2017).
[11] De Mitri I., EPJ Web of Conferences, **136** , 02010 (2017).